Noise-Robust Distributed Quantum Sensing: A Variational Quantum Approach

Uman Khalid*, Muhammad Shohibul Ulum*, Trung Q. Duong†, Moe Z. Win‡, and Hyundong Shin*
*Department of Electronics and Information Convergence Engineering, Kyung Hee University, Republic of Korea
†Faculty of Engineering and Applied Science, Memorial University, St. John's, NL A1C 5S7, Canada
†School of Electronics, Electrical Engineering and Computer Science, Queen's University Belfast, Belfast, U.K.
‡Laboratory for Information and Decision Systems, Massachusetts Institute of Technology, Cambridge, MA 02139 USA
Email: {umankhalid, msulum, hshin}@khu.ac.kr, tduong@mun.ca, moewin@mit.edu

***Abstract*—Quantum sensing networks (QSNs) are expected to play a critical role in quantum networks by achieving measurement precision unattainable with classical methods, leveraging quantum properties such as superposition and entanglement. Distributed quantum sensing, a key application of QSNs, can reach Heisenberg-limited precision scaling with the number of sensors involved. However, practical implementation faces significant challenges due to noise effects, complicating the optimal selection of sensor configurations. In this paper, we propose applying a variational quantum algorithm (VQA) combined with a genetic algorithm to efficiently mitigate noise in quantum sensing protocols and to identify high-quality sensor configurations. Performance analysis demonstrates that our approach outperforms traditional sensor configuration methods in single- and multi-parameter sensing scenarios under dephasing and amplitude damping noises, significantly improving quantum sensing accuracy and scalability.**

***Index Terms*—Distributed quantum sensing, quantum sensing networks, variational quantum sensing.**

I. Introduction

Quantum information science provides unique advantages across computing, communication, and sensing by leveraging quantum properties like superposition and entanglement. Quantum computing enables solving computationally challenging problems beyond classical methods by exploiting quantum parallelism and entanglement [1]. Quantum communication offers secure information exchange over entangled networks, guaranteeing unconditional security against eavesdropping [2]. Meanwhile, quantum sensing achieves measurement precision unattainable classically by using entangled sensor networks to collaboratively measure physical quantities at Heisenberg-limit scaling [3].

Currently, quantum devices operate within the noisy intermediate-scale quantum (NISQ) era, limiting their practicality, scalability, and performance [4]. To effectively utilize NISQ devices, variational quantum algorithms (VQAs) have emerged as promising technique as they optimize quantum circuit parameters iteratively using classical optimization methods and quantum measurements, enabling efficient use of quantum resources despite limited hardware capabilities. This class of algorithms has already demonstrated effectiveness across diverse applications, including machine learning, combinatorial optimization, and mathematical modeling [5].

Quantum sensing leverages entangled sensor nodes (SNs) to achieve precision scaling unattainable by classical methods, approaching the fundamental Heisenberg limit. However, environmental noise significantly impacts sensing precision by degrading entangled quantum states [6]. To mitigate this, VQAs can tailor quantum probe states specifically for noisy environments, preserving quantum advantages. By optimizing quantum states with classical optimization techniques, variational quantum sensing can effectively counteract noise-induced degradation, thus achieving higher sensing precision than classical methods [7].

In this paper, we integrate quantum computing techniques into distributed quantum sensing protocols within quantum networks to effectively mitigate environmental noise. Specifically, we introduce a quantum computing-based variational approach to optimize quantum sensing protocols tailored to spatially distributed sensing scenarios. Recognizing the complexity of identifying an optimal ansatz structure within a vast search space, we employ a genetic algorithm to efficiently select high-quality ansatz configurations. Subsequently, the chosen ansatz structures are optimized via classical optimization methods tailored to single- and multi-parameter sensing scenarios. The performance of the proposed approach is rigorously evaluated using the quantum Cramér–Rao bound (QCRB), highlighting improvements in noise mitigation and precision scalability for distributed quantum sensing applications.

The rest of the paper is organized as follows. Section II introduces fundamental concepts of quantum sensing and VQAs. Section III presents a variational distributed quantum sensing framework, integrating variational state preparation, that leverages genetic algorithms for ansatz optimization, with distributed sensing protocols. Section IV provides numerical analyses and performance evaluations for single- and multi-parameter sensing scenarios under realistic noise conditions, specifically dephasing and amplitude damping, quantified via the QCRB. Section V concludes this work.

II. Preliminary

We first review fundamental concept regarding quantum sensing and VQAs.

A. Quantum Sensing

Typically, quantum sensing follows a series of protocol steps which utilize quantum resources to achieve enhanced sensing precision scaling.

1) Protocol: Quantum sensing protocol starts by preparing the sensing probe state $|\boldsymbol{\psi}\rangle$. The quantity to be sensed $\boldsymbol{\zeta} = (\zeta_1, \zeta_2, \cdots, \zeta_K)$ having K unknown parameters is then encoded into this sensing probe state using a unitary operation that is generated by Hamiltonian $\tilde{\boldsymbol{\mathcal{H}}} = (\boldsymbol{\mathcal{H}}_1, \boldsymbol{\mathcal{H}}_2, \cdots, \boldsymbol{\mathcal{H}}_K)$ as

$$\boldsymbol{U}\left(\tilde{\boldsymbol{\mathcal{H}}}; \boldsymbol{\zeta}\right) = \exp\left(-\imath \tilde{\boldsymbol{\mathcal{H}}} \cdot \boldsymbol{\zeta}\right) \tag{1}$$

where $\imath = \sqrt{-1}$ and the encoding evolution takes the form of $|\boldsymbol{\psi}(\boldsymbol{\zeta})\rangle = \boldsymbol{U}\left(\tilde{\boldsymbol{\mathcal{H}}}; \boldsymbol{\zeta}\right)|\boldsymbol{\psi}\rangle$. The encoded probe state $|\boldsymbol{\psi}(\boldsymbol{\zeta})\rangle$ is then measured with a set of measurement basis $\{|\boldsymbol{\phi}_i\rangle\}$. Based on the measurement outcome i, the quantity $\boldsymbol{\zeta}$ is estimated. The aim of the quantum sensing protocol is to find the optimal probe state $|\boldsymbol{\psi}\rangle$ and measurement basis $\{|\boldsymbol{\phi}_i\rangle\}$ to estimate the quantity $\boldsymbol{\zeta}$ with the best possible precision.

2) Precision: The precision to estimate $\boldsymbol{\zeta}$ using unbiased estimator $\hat{\boldsymbol{\zeta}}$ can be quantified using quantum Fisher information (QFI) which is originally defined as [8]

$$\mathcal{I}_{ij}\left(\boldsymbol{\rho}(\boldsymbol{\zeta})\right) = \frac{1}{2}\operatorname{tr}\left(\boldsymbol{\rho}(\boldsymbol{\zeta})\left\{\boldsymbol{\Lambda}_i, \boldsymbol{\Lambda}_j\right\}\right) \tag{2}$$

where $\boldsymbol{\rho}$ is the density matrix representation of a quantum state which is a linear combination of $\{|\psi_i\rangle\langle\psi_i|\}$ for an orthogonal basis $\{|\psi_i\rangle\}$ and has trace of 1, $\{\boldsymbol{A}, \boldsymbol{B}\} = \boldsymbol{AB} + \boldsymbol{BA}$ is the anti-commutator, and the operator $\boldsymbol{\Lambda}_i$ is the symmetric logarithmic derivative for the parameter ζ_i, defined implicitly as

$$\partial_{\zeta_i}\boldsymbol{\rho}(\boldsymbol{\zeta}) = \frac{1}{2}\left\{\boldsymbol{\Lambda}_i, \boldsymbol{\rho}(\boldsymbol{\zeta})\right\}, \tag{3}$$

where $\partial_{\zeta_i}\boldsymbol{\rho}(\boldsymbol{\zeta})$ is the derivative of $\boldsymbol{\rho}(\boldsymbol{\zeta})$ with respect to ζ_i. For the encoded probe state $\boldsymbol{\rho}(\boldsymbol{\zeta}) = |\boldsymbol{\psi}(\boldsymbol{\zeta})\rangle\langle\boldsymbol{\psi}(\boldsymbol{\zeta})|$, the (i,j)th element of the QFI $\boldsymbol{\mathcal{I}}(\boldsymbol{\rho}(\boldsymbol{\zeta}))$ is given by [8]

$$\begin{aligned}\mathcal{I}_{ij}\left(\boldsymbol{\rho}(\boldsymbol{\zeta})\right) =& 2\langle\boldsymbol{\psi}|\left\{\boldsymbol{\mathcal{H}}_i, \boldsymbol{\mathcal{H}}_j\right\}|\boldsymbol{\psi}\rangle \\ &- 4\langle\boldsymbol{\psi}|\boldsymbol{\mathcal{H}}_i|\boldsymbol{\psi}\rangle\langle\boldsymbol{\psi}|\boldsymbol{\mathcal{H}}_j|\boldsymbol{\psi}\rangle,\end{aligned} \tag{4}$$

which depends only on the probe state $|\boldsymbol{\psi}\rangle$. The QFI can also be related to the quantum state fidelity as follows [9]:

$$\boldsymbol{\zeta}\boldsymbol{\mathcal{I}}(\boldsymbol{\rho})\boldsymbol{\zeta}^T \approx 8\|\boldsymbol{\zeta}\|^2\left(\frac{1-\sqrt{f\left(\boldsymbol{\rho}, \boldsymbol{\rho}\left(\epsilon\boldsymbol{\zeta}/\|\boldsymbol{\zeta}\|\right)\right)}}{\epsilon^2}\right) \tag{5}$$

where T is the transpose operator, $\epsilon \ll 1$ is a small real number, and fidelity between two quantum states $\boldsymbol{\rho}$ and $\boldsymbol{\sigma}$ is given by $f(\boldsymbol{\rho}, \boldsymbol{\sigma}) = \left(\operatorname{tr}\sqrt{\sqrt{\boldsymbol{\rho}}\boldsymbol{\sigma}\sqrt{\boldsymbol{\rho}}}\right)^2$. Using the QFI, the total variance of the unbiased estimator $\hat{\boldsymbol{\zeta}}$ is bounded by QCRB as

$$\operatorname{tr}\left(\operatorname{Cov}\left[\hat{\boldsymbol{\zeta}}\right]\right) = \sum_{k=1}^{K}\operatorname{Var}\left[\hat{\zeta}_k\right] \geq \operatorname{tr}\left[\boldsymbol{\mathcal{I}}^{-1}(\boldsymbol{\rho})\right]. \tag{6}$$

where $\operatorname{Cov}\left[\hat{\boldsymbol{\zeta}}\right]$ is the covariance matrix of $\hat{\boldsymbol{\zeta}}$.

B. Variational Quantum Algorithms

VQAs generate candidate solutions using quantum computers via ansatz structures composed of parameterized quantum gates, iteratively refining solutions by evaluating a classical cost function optimized classically, thus efficiently navigating toward optimal solutions.

1) Ansatz Structure: The quantum gates within the ansatz can be categorized as single-qubit gates and entangling gates which both can be written as parameterized unitary operator

$$\boldsymbol{U}(\boldsymbol{\mathcal{O}}; \theta) = \exp\left(-\imath\boldsymbol{\mathcal{O}}\theta\right), \tag{7}$$

where for single-qubit gates $\boldsymbol{\mathcal{O}}$ is a local Hamiltonian, for entangling gates $\boldsymbol{\mathcal{O}}$ consist of interacting Hamiltonian that act on more than one qubit, and θ is the gate's parameter. One special case of entangling gates can also be written in the controlled form as,

$$\boldsymbol{U}(\boldsymbol{\mathcal{O}}; \theta) = |0\rangle\langle 0| \otimes \boldsymbol{I} + |1\rangle\langle 1| \otimes \exp\left(-\imath\boldsymbol{\mathcal{O}}\theta\right), \tag{8}$$

where $\boldsymbol{\mathcal{O}}$ is a local Hamiltonian, $\otimes$ is the tensor product, and $\boldsymbol{I}$ is the identity operator. This controlled gates will perform $\exp\left(-\imath\boldsymbol{\mathcal{O}}\theta\right)$ to the target qubit if the control qubit in the state $|1\rangle$ and leave the target qubit unchanged, otherwise. In general, the ansatz can be written as a series of L parameterized unitary

$$\boldsymbol{U}\left(\tilde{\boldsymbol{\mathcal{O}}}; \boldsymbol{\theta}\right) = \boldsymbol{U}(\boldsymbol{\mathcal{O}}_L; \theta_L)\cdots\boldsymbol{U}(\boldsymbol{\mathcal{O}}_2; \theta_2)\boldsymbol{U}(\boldsymbol{\mathcal{O}}_1; \theta_1), \tag{9}$$

where $\boldsymbol{\theta} = (\theta_1, \theta_2, \ldots, \theta_L)$ is the ansatz parameters to be optimized and $\tilde{\boldsymbol{\mathcal{O}}} = (\boldsymbol{\mathcal{O}}_1, \boldsymbol{\mathcal{O}}_2, \ldots, \boldsymbol{\mathcal{O}}_L)$.

2) Cost Function: The potential solution $|\boldsymbol{\psi}(\boldsymbol{\theta})\rangle$ is obtained by the action of the ansatz $\boldsymbol{U}\left(\tilde{\boldsymbol{\mathcal{O}}}; \boldsymbol{\theta}\right)$ on the initial states $|\boldsymbol{\psi}\rangle$ as

$$|\boldsymbol{\psi}(\boldsymbol{\theta})\rangle = \boldsymbol{U}\left(\tilde{\boldsymbol{\mathcal{O}}}; \boldsymbol{\theta}\right)|\boldsymbol{\psi}\rangle. \tag{10}$$

This potential solution is evaluated using the cost function that can be written in the form of,

$$C(\boldsymbol{\theta}) = g\left(\{|\boldsymbol{\phi}_i\rangle\}, |\boldsymbol{\psi}(\boldsymbol{\theta})\rangle\right) \tag{11}$$

where g is a real-valued function and $\{|\boldsymbol{\phi}_i\rangle\}$ is the measurement basis. The cost function should accurately encode the problem of interest and can be trained using classical computer. The quality of the potential solution should be improve as the cost function optimized and the best solution should corresponds to the optimal cost function. In the following framework, the genetic algorithm (GA)'s fitness criterion is explicitly defined to maximize the QFI, thereby ensuring that the ansatz structures remain directly aligned with the sensing task [7], [10].

3) Classical Optimizer: The goal of the classical optimizer is to find the optimal ansatz parameters

$$\boldsymbol{\theta}_\star = \arg\min C(\boldsymbol{\theta}) \tag{12}$$

such that $|\boldsymbol{\psi}(\boldsymbol{\theta}_\star)\rangle$ corresponds to the best solution. In small number of ansatz parameters, the gradient-based optimizers are preferable that use the gradient of the cost function

TABLE I
QCRBs FOR 0.05 DECAY RATE

Scenario	Sensing Nodes	x-dephasing		z-dephasing		Amplitude Damping	
		GHZ	VPS	GHZ	VPS	GHZ	VPS
Single-parameter	2	0.01500	0.00888	0.01289	0.00917	0.00516	0.00285
	3	0.01046	0.00662	0.01046	0.00574	0.00468	0.00221
	4	0.00839	0.00411	0.00851	0.00415	0.00460	0.00148
	5	0.00723	0.00372	0.00745	0.00312	0.00442	0.00112
Multi-parameter	2	0.12628	0.07984	0.09935	0.07984	0.03166	0.02423
	3	0.07463	0.04902	0.08678	0.04861	0.01989	0.01829
	4	0.04361	0.03854	0.04712	0.03967	0.01592	0.01395
	5	0.03378	0.03138	0.03760	0.03188	0.01163	0.01090

to guide the optimizers to minimize the cost function. In VQAs, one can use parameter-shift rule to calculate the gradient of the cost function [11]. Common gradient-based optimizers used in VQAs are stochastic gradient descent and Adam optimizer [12], [13]. As the number of ansatz parameters grows, the VQAs face trainability problems as the gradient are vanishing at exponential rate and the number of local optima are rising [14]. In this case, gradient-free optimizers become more popular as it does not rely on the gradient to optimize the cost function. Common gradient-free optimzers used in VQAs includes the constrained optimization by linear approximations (COBYLA), Broyden-Fletcher-Goldfarb-Shanno (BFGS), and evolutionary algorithms [15], [16]. While gradient-free optimizers cannot universally avoid barren plateaus [9], [14], in the NISQ regime they provide practical robustness against vanishing gradients by maintaining stable updates in moderate-dimensional parameter spaces, as also observed in evolutionary-optimization studies [16].

III. Variational Distributed Quantum Sensing

Herein, we combine variational state preparation and distributed sensing protocol over quantum sensing networks (QSNs) to mitigate noise effects.

A. Variational State Preparation

1) Genetic Quantum Circuit: The structure of the ansatz dictates how good the circuit exploring the quantum states in the Hilbert space. To deal with the huge ansatz structure space, GA can be used to find the ansatz structure heuristically [10]. The GA consist of a population of ansatz structures that are represented by chromosomes. The chromosomes consist of genes which is constructed as,

$$\mathfrak{g} = (\boldsymbol{\mathcal{O}}, |c\rangle, |t\rangle, \theta), \tag{13}$$

where $\boldsymbol{\mathcal{O}}$ is a local Hamiltonian taken from a set $\{\boldsymbol{\sigma}_{\mathrm{x}}, \boldsymbol{\sigma}_{\mathrm{y}}, \boldsymbol{\sigma}_{\mathrm{z}}\}$, $\boldsymbol{\sigma}_{\mathrm{x}} = |1\rangle\langle 0| + |0\rangle\langle 1|$, $\boldsymbol{\sigma}_{\mathrm{z}} = |0\rangle\langle 0| - |1\rangle\langle 1|$, $\boldsymbol{\sigma}_{\mathrm{y}} = \imath\boldsymbol{\sigma}_{\mathrm{x}}\boldsymbol{\sigma}_{\mathrm{z}}$, $|c\rangle$ is the control qubit, $|t\rangle$ is the target qubit, and θ is the parameter. This gene is then mapped into the parameterized unitary as

$$\mathcal{M}(\mathfrak{g}) = \exp(-\imath\boldsymbol{\mathcal{O}}\theta) \tag{14}$$

for local gate which acts on the target qubit $|t\rangle$ and

$$\mathcal{M}(\mathfrak{g}) = |0\rangle\langle 0| \otimes \boldsymbol{I} + |1\rangle\langle 1| \otimes \exp(-\imath\boldsymbol{\mathcal{O}}\theta) \tag{15}$$

is the controlled gate which acts on the control and target qubits $|c\rangle \otimes |t\rangle$.

The chromosome having L number of genes is evaluated using the fitness function on the resulted state

$$|\boldsymbol{\psi}(\boldsymbol{\theta})\rangle = \mathcal{M}(\mathfrak{g}_L) \cdots \mathcal{M}(\mathfrak{g}_2)\, \mathcal{M}(\mathfrak{g}_1)\, |\boldsymbol{\psi}\rangle. \tag{16}$$

Parent chromosomes for generating the next population are selected based on fitness using either elitism (choosing the single fittest chromosome) or tournament selection (selecting the top r chromosomes out of a randomly chosen subset of s). Next-generation chromosomes are produced via genetic operations: gene deletion (removing a sequence of genes), gene insertion (adding a random gene sequence), and gene replacement (combining deletion and insertion sequentially). These evolutionary strategies efficiently navigate the large ansatz search space, optimizing quantum sensing configurations.

2) Circuit Optimization: After the ansatz is found by the genetic algorithm, the parameters in the ansatz are further optimized using classical optimizer. The optimization is performed based on the QFI that acts as a cost function. The QFI is approximated by the distance traveled by the variational state $\boldsymbol{\rho}(\boldsymbol{\theta}) = |\boldsymbol{\psi}(\boldsymbol{\theta})\rangle\langle\boldsymbol{\psi}(\boldsymbol{\theta})|$ when small unknown quantity $\epsilon\boldsymbol{e}_k$ is encoded in the $\boldsymbol{\rho}(\boldsymbol{\theta})$ as given by

$$\mathcal{I}_{kk}(\boldsymbol{\rho}(\boldsymbol{\theta})) \approx 8\left(\frac{1 - \sqrt{f(\boldsymbol{\rho}(\boldsymbol{\theta}), \boldsymbol{\rho}(\boldsymbol{\theta}; \epsilon\boldsymbol{e}_k))}}{\epsilon^2}\right), \tag{17}$$

$$\mathcal{I}_{ij}(\boldsymbol{\rho}(\boldsymbol{\theta})) \approx 4\left(\frac{1 - \sqrt{f(\boldsymbol{\rho}(\boldsymbol{\theta}), \boldsymbol{\rho}(\boldsymbol{\theta}; \epsilon\boldsymbol{e}_i + \epsilon\boldsymbol{e}_j))}}{\epsilon^2}\right) - \frac{\mathcal{I}_{ii}(\boldsymbol{\rho}(\boldsymbol{\theta})) + \mathcal{I}_{jj}(\boldsymbol{\rho}(\boldsymbol{\theta}))}{2}, \tag{18}$$

and $\mathcal{I}_{ij}(\boldsymbol{\rho}(\boldsymbol{\theta})) = \mathcal{I}_{ji}(\boldsymbol{\rho}(\boldsymbol{\theta}))$ due to the symmetric property of the QFI, where $\boldsymbol{e}_k$ is the kth row of the identity operator in the parameter space. The cost function is taken as the

$$C(\boldsymbol{\theta}) = \mathrm{tr}\left[\boldsymbol{\mathcal{I}}(\boldsymbol{\rho}(\boldsymbol{\theta}))^{-1}\right]. \tag{19}$$

Gradient-free optimizer is then used to optimize the cost function $C(\boldsymbol{\theta})$.

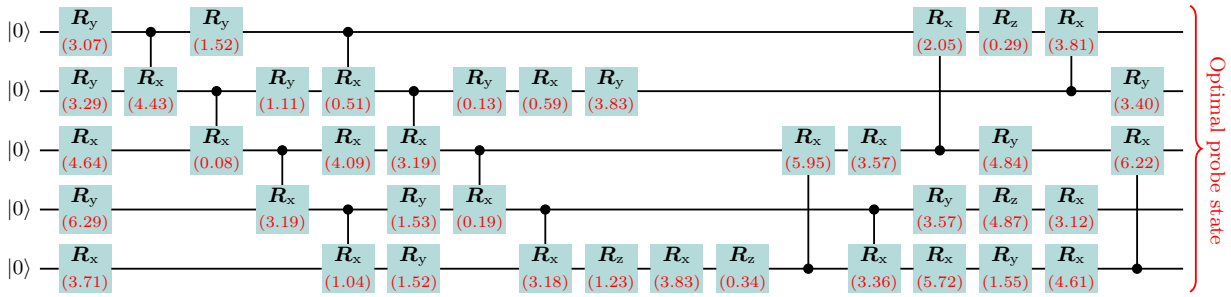

Fig. 1. Optimized ansatz in single-parameter scenario for $N = 5$ under x-direction dephasing noise.

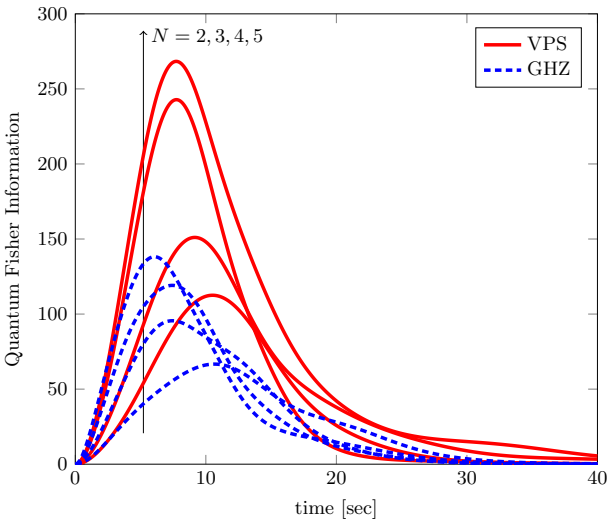

Fig. 2. Quantum Fisher Information in single-parameter scenario under x-direction dephasing noise.

B. Distributed Sensing Protocol

1) Probe Distribution: The distributed quantum sensing protocol starts with distributing the prepared variational probe state (VPS) $|\psi(\boldsymbol{\theta})\rangle$ by computing node (CN) to the spatially separated SNs. The distribution is accomplished by means of quantum teleportation via preshared entanglement channels between the CN and distant SNs. The preshared entanglement channels are in the form of Bell states, maximally two-qubits entangled states, $|\mathsf{Bell}\rangle = (|00\rangle + |11\rangle)/\sqrt{2}$ where the CN and SNs keep their respective shared qubit. To teleport the ith qubit VPS to the ith SN, the CN performs joint measurement of the ith qubit $|\psi(\boldsymbol{\theta})\rangle$ and its respective shared qubit of preshared Bell state with the ith SN in Bell basis $|\mathbf{m}\rangle = \left(|0\mathsf{m}_1\rangle + (-1)^{\mathsf{m}_0}|1\bar{\mathsf{m}}_1\rangle\right)/\sqrt{2}$, where $\mathbf{m} \in \{0,1\}^2$ and $\bar{\mathsf{m}}_1 = 1 - \mathsf{m}_1$. The CN then sends the measurement outcome $\mathbf{m}$ to notify the ith SN for required recovery operations. Upon receiving $\mathbf{m}$, the ith SN apply $\boldsymbol{\sigma}_{\mathsf{z}}^{\mathsf{m}_0}\boldsymbol{\sigma}_{\mathsf{x}}^{\mathsf{m}_1}$ on its shared qubit to conclude the ith qubit VPS teleportation. Such teleportation procedure is carried for all qubits in $|\psi(\boldsymbol{\theta})\rangle$ to respective SNs to complete the VPS distribution.

2) Probe Parameterization: The ith SN lets its VPS qubit interacts with the local unknown quantity $\boldsymbol{\zeta}_i = (\zeta_{i1}, \zeta_{i2}, \cdots, \zeta_{iK})$ having K unknown components by encoding $\boldsymbol{\zeta}_i$ to the VPS via Hamiltonian $\tilde{\boldsymbol{\mathcal{H}}}_i = (\boldsymbol{\mathcal{H}}_{i1}, \boldsymbol{\mathcal{H}}_{i2}, \cdots, \boldsymbol{\mathcal{H}}_{iK})$ by unitary operator

$$\boldsymbol{U}\left(\tilde{\boldsymbol{\mathcal{H}}}_i; \boldsymbol{\zeta}_i\right) = \exp\left(-\imath\tilde{\boldsymbol{\mathcal{H}}}_i \cdot \boldsymbol{\zeta}_i\right) \tag{20}$$

where $\boldsymbol{\mathcal{H}}_{ik}$ is the Hamiltonian that encodes the kth unknown component at the ith SN. All SNs perform such parameterization to encode their respective local unknown quantity in their respective VPS qubit governed by the local Hamiltonian.

3) Parameter Estimation: The encoded quantities are extracted from the encoded VPS by means of quantum measurement by the CN enabling joint global measurement to be employed. Hence, similar quantum state teleportation protocol as in the probe distribution step will be carried. Herein, the SNs will perform the Bell basis measurement on its encoded qubit and shared Bell state qubit. The SNs send the measurement outcome to CN. The CN will perform recovery operation based on the received measurement outcome. After all encoded VPS qubits are teleported to the CN, it prepares the measurement basis $\{|\phi_i\rangle\}$ and perform the measurement on the encoded VPS with that basis to extract maximal information of the encoded quantities. The measurement outcomes are then used to estimate the global properties of the local quantities.

IV. Numerical Results

To simulate noisy quantum sensing scenario, we use Lindblad master equation that describes Markovian interaction between the quantum sensing system and environment where the reduced system evolution is given by

$$\frac{d\boldsymbol{\rho}(t)}{dt} = -\imath\left[\boldsymbol{\mathcal{H}}, \boldsymbol{\rho}(t)\right] + \boldsymbol{\mathcal{L}}\left(\boldsymbol{\rho}(t)\right) \tag{21}$$

with

$$\boldsymbol{\mathcal{L}}\left(\boldsymbol{\rho}(t)\right) = \sum_{i=1}^{N}\gamma_i\left(\boldsymbol{\Gamma}_i\boldsymbol{\rho}(t)\boldsymbol{\Gamma}_i^{\dagger} - \frac{1}{2}\left\{\boldsymbol{\Gamma}_i^{\dagger}\boldsymbol{\Gamma}_i, \boldsymbol{\rho}(t)\right\}\right) \tag{22}$$

where $[\boldsymbol{A}, \boldsymbol{B}] = \boldsymbol{A}\boldsymbol{B} - \boldsymbol{B}\boldsymbol{A}$, γ_i is the decay rate, and $\boldsymbol{\Gamma}_i$ is the decay operator for the ith SN. The first term in the master equation (21) corresponds to closed quantum system where there are no interaction with the environment and the dynamics is in the form of unitary operator, whereas the second term $\boldsymbol{\mathcal{L}}(\boldsymbol{\rho}(t))$ relates to the open quantum system

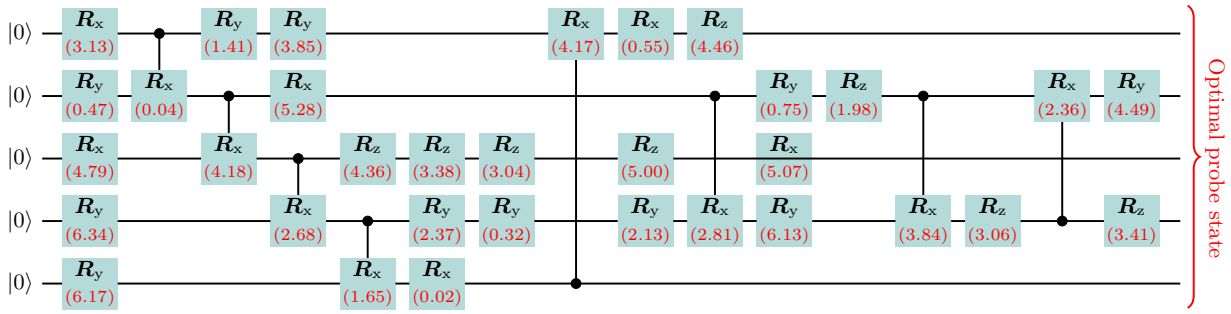

Fig. 3. Optimized ansatz in multi-parameter scenario for $N = 5$ under x-direction dephasing noise.

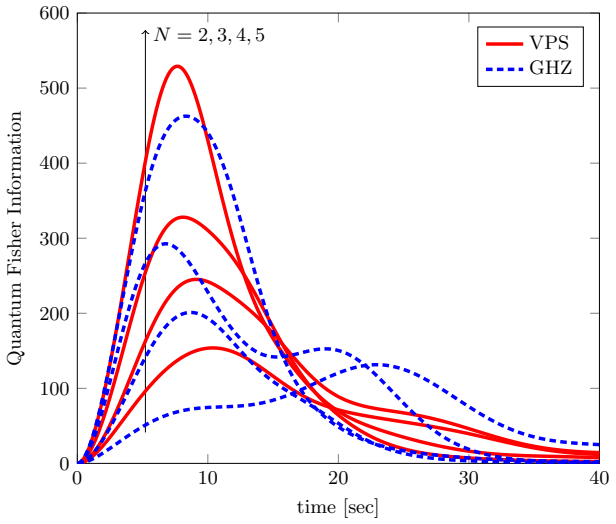

Fig. 4. Quantum Fisher Information in multi-parameter scenario under x-direction dephasing noise.

where interaction between the system and environment exist which result in non-unitary dynamics.

We consider three anisotropic quantum noises, namely dephasing in x-direction, dephasing in z-direction, and amplitude damping. For dephasing in $\mathrm{w} \in \{\mathrm{x}, \mathrm{z}\}$-direction, the decay operator for ith SN is given by

$$\boldsymbol{\Gamma}_i = \boldsymbol{I}^{\otimes(i-1)} \otimes \boldsymbol{\sigma}_{\mathrm{w}} \otimes \boldsymbol{I}^{\otimes(N-i)}. \tag{23}$$

Here, N represents the number of distributed sensing nodes (or equivalently, qubits) participating in the variational probe state, consistent with standard treatments of distributed quantum sensing in noisy environments [7], [8]. The non-unitary dynamics $\boldsymbol{\mathcal{L}}(\boldsymbol{\rho}(t))$ for the w-direction dephasing noise is then given by

$$\boldsymbol{\mathcal{L}}(\boldsymbol{\rho}(t)) = \sum_{i=1}^{N} \gamma_i \left(\boldsymbol{\Gamma}_i \boldsymbol{\rho}(t) \boldsymbol{\Gamma}_i - \boldsymbol{\rho}(t)\right). \tag{24}$$

For amplitude damping, the decay operator for ith SN is given by

$$\boldsymbol{\Gamma}_i = \boldsymbol{I}^{\otimes(i-1)} \otimes \boldsymbol{\sigma}_{\mathrm{xy}} \otimes \boldsymbol{I}^{\otimes(N-i)}. \tag{25}$$

where $\boldsymbol{\sigma}_{\mathrm{xy}} = (\boldsymbol{\sigma}_{\mathrm{x}} + \imath\boldsymbol{\sigma}_{\mathrm{y}})/2$.

We consider the sensing of magnetic field where we assume that each SN encodes the magnetic field with the same value $\boldsymbol{\zeta}_i = (\zeta_1, \zeta_2, \zeta_3) = \boldsymbol{\zeta}_j$. The CN then aims to estimate the average of the magnetic field $\boldsymbol{\zeta} = \frac{1}{N}\sum_i \boldsymbol{\zeta}_i = (\zeta_1, \zeta_2, \zeta_3)$. Each SN encodes its magnetic field using the Hamiltonian $\tilde{\boldsymbol{\mathcal{H}}}_i = (\boldsymbol{\sigma}_{\mathrm{x}}, \boldsymbol{\sigma}_{\mathrm{y}}, \boldsymbol{\sigma}_{\mathrm{z}})/2$ which generates encoding unitary

$$\boldsymbol{U}\left(\tilde{\boldsymbol{\mathcal{H}}}_i; \boldsymbol{\zeta}\right) = \exp\left[-\frac{\imath}{2}\left(\boldsymbol{\sigma}_{\mathrm{x}}\zeta_1 + \boldsymbol{\sigma}_{\mathrm{y}}\zeta_2 + \boldsymbol{\sigma}_{\mathrm{z}}\zeta_3\right)\right]. \tag{26}$$

In both single- and multi-parameter sensing scenarios, we consider perfect teleportation protocol where the fidelity of input and output state of the teleportation protocol is unity.

A. Single-parameter Sensing

For single-parameter sensing scenario, the encoding unitary can be written as $\boldsymbol{U}\left(\tilde{\boldsymbol{\mathcal{H}}}_i; \boldsymbol{\zeta}\right) = \boldsymbol{U}\left(\hat{\boldsymbol{\mathcal{H}}}_i; \|\boldsymbol{\zeta}\|\right) = \exp\left(-\imath\hat{\boldsymbol{\mathcal{H}}}_i\|\boldsymbol{\zeta}\|\right)$ where $\hat{\boldsymbol{\mathcal{H}}}_i = \left(\boldsymbol{\sigma}_{\mathrm{x}}\zeta_1 + \boldsymbol{\sigma}_{\mathrm{y}}\zeta_2 + \boldsymbol{\sigma}_{\mathrm{z}}\zeta_3\right)/\left(2\|\boldsymbol{\zeta}\|\right)$. Then, the aim of the single-parameter sensing is to sense the magnitude of the magnetic field $\|\boldsymbol{\zeta}\|$. In noiseless sensing scenario, the optimal probe state for single-parameter sensing is the Greenberger–Horne–Zeilinger (GHZ)-type state in the basis of the encoding Hamiltonian $\hat{\boldsymbol{\mathcal{H}}}_i$. Let $|\lambda_{ij}\rangle$ be the eigenvectors of the Hamiltonian $\hat{\boldsymbol{\mathcal{H}}}_i$ for $j \in \{0, 1\}$, then the optimal probe state for the noiseless scenario is given by

$$|\mathsf{sp}\rangle = \frac{1}{\sqrt{2}}\left(|\lambda_{10}\rangle|\lambda_{20}\rangle\cdots|\lambda_{N0}\rangle + |\lambda_{11}\rangle|\lambda_{21}\rangle\cdots|\lambda_{N1}\rangle\right) \tag{27}$$

where all SNs can be seen as a global system that has a maximally entangled state in the $\hat{\boldsymbol{\mathcal{H}}}_i$ eigenvectors basis $\{|\lambda_{ij}\rangle\}$. This $|\mathsf{sp}\rangle$ is the most sensitive state for the encoding unitary $\boldsymbol{U}\left(\hat{\boldsymbol{\mathcal{H}}}_i; \|\boldsymbol{\zeta}\|\right)$. However it may also very sensitive to noises so that its sensitivity to the parameter is beaten by the sensitivity to noises rendering the information about the parameter are no longer encoded optimally. There may exist other probe states that can encode more information about $\|\boldsymbol{\zeta}\|$ in the presence of noises.

We simulate this single-parameter sensing scenario for $N = \{2, 3, 4, 5\}$ SNs under x-direction dephasing, z-direction dephasing, and amplitude damping noises. The decay rate for each SN is set to $\gamma_i = 0.05$. The VPS state is obtained by

finding the ansatz by the genetic algorithm with the QFI as the fitness function. The ansatz consists of single-qubit rotation gates $\boldsymbol{R}_{\mathrm{v}}(\theta) = \exp(-\imath\boldsymbol{\sigma}_{\mathrm{v}}\theta/2)$ and two-qubit controlled-$\boldsymbol{R}_{\mathrm{x}}(\theta)$ gates, where $\mathrm{v} \in \{\mathrm{x},\mathrm{y},\mathrm{z}\}$ and $\theta \in [0, 2\pi]$. After the ansatz structure is found, the ansatz parameters are further optimized based on the QFI.

The result is shown in Table I where the performance of VPS and GHZ are compared using QCRB. It is shown that for $N = \{2,3,4,5\}$ the VPS outperforms the GHZ state by achieving lower QCRB for x-direction dephasing, z-direction dephasing, and amplitude damping noises. It can also be seen that, the more SNs involved in the distributed scenario, the better is the performance as it achieve lower QCRB as the number of SNs involved grows. Furthermore, both GHZ and VPS are more robust in amplitude damping noise as compared to the dephasing noises for all $N = \{2,3,4,5\}$.

Fig. 1 and 2 show the optimized ansatz and the QFI dynamics under x-direction dephasing noise, respectively. Fig. 1 shows the genetically searched ansatz structure alongside the optimal ansatz parameters that are optimized with classical optimizer for $N = 5$ SNs. Fig. 2 shows the QFI dynamics across time for both VPS and GHZ for all $N = \{2,3,4,5\}$. For each N, the VPS reaches higher maximum QFI value as compared to GHZ. Although the VPS reaches maximum QFI value at slightly later time as compared to GHZ, the maximum QFI value achieved by VPS is significantly more than what achieved by GHZ.

B. Multi-parameter Sensing

For multi-parameter scenario, the aim is to sense all component of $\boldsymbol{\zeta}$ simultaneously. In contrast with single-parameter scenario, the optimal probe state for multi-parameter, in general, is not analytically known even for the noiseless case. For three-dimensional magnetic field, as considered in this scenario, probe states in the form of

$$|\boldsymbol{\psi}(\boldsymbol{\theta})\rangle = \frac{|\boldsymbol{\phi}(\boldsymbol{\theta})\rangle}{\| |\boldsymbol{\phi}(\boldsymbol{\theta})\rangle \|} \tag{28}$$

where

$$|\boldsymbol{\phi}(\boldsymbol{\theta})\rangle = \frac{1}{\sqrt{2}} \sum_{\mathrm{v}} e^{-\imath\theta_{\mathrm{v}}} \left(|\lambda_0\rangle_{\mathrm{v}}^{\otimes N} + |\lambda_1\rangle_{\mathrm{v}}^{\otimes N} \right) \tag{29}$$

having $\{|\lambda_i\rangle_{\mathrm{v}}\}$ is the eigenbasis of the Hamiltonian $\boldsymbol{\sigma}_{\mathrm{v}}$ and $\boldsymbol{\theta} = (\theta_{\mathrm{x}}, \theta_{\mathrm{y}}, \theta_{\mathrm{z}})$ reach Heisenberg precision scaling [17]. We will simply call the probe state in (28) a GHZ state.

Similar with the GHZ state in the single-parameter case, this GHZ state can also be outperformed by the other probe states in noisy sensing scenario. As shown in Table I, the tailored VPS outperforms the GHZ state for all $N = \{2,3,4,5\}$ under x-direction dephasing, z-direction dephasing, and amplitude damping noises. Here, we also optimized the parameters in the GHZ state $|\boldsymbol{\phi}(\boldsymbol{\theta})\rangle$. The VPS performance improve as more SNs involved in the sensing task. Moreover, like in single-parameter scenario, both VPS and GHZ are more robust to amplitude damping as compared to dephasing noises.

Fig. 3 and 4 show the optimized ansatz and the QFI dynamics under x-direction dephasing noise, respectively. Fig. 3 shows the genetic ansatz structure with its optimized ansatz parameters for $N = 5$ SNs. Fig. 4 shows the QFI dynamics over time where the QFI is taken as the summation of all the QFI matrix elements. This quantify the sensitivity of the probe state when perturb by small changes of parameters $\epsilon\boldsymbol{\zeta}$ for small $\epsilon > 0$. As shown in the Fig. 4, VPS can achieve higher maximum QFI value as compared to the GHZ state with better maximum QFI value and time to reach the maximum QFI value ratio for all $N = \{2,3,4,5\}$. This indicates that the VPS is more sensitive as compared to GHZ state to the small change of the parameters to be sensed. Moreover, the smaller QFI advantage of VPS over GHZ in the multi-parameter case arises because simultaneous estimation involves non-commuting observables and cross-parameter correlations, which complicate optimization and limit ansatz expressiveness [8], [17].

V. Conclusion

Distributed sensing is a promising application in QSNs, as it leverages quantum correlations to achieve measurement precision beyond classical limits. However, traditional quantum states like the GHZ state, while powerful, are vulnerable to environmental noise, which significantly reduces their effectiveness in realistic scenarios. To overcome this, we employ a genetically tailored ansatz structure with optimized parameters to identify quantum probe states that maximize metrological precision under noisy conditions. The resulting optimized VPS outperform standard GHZ states across various sensing scenarios. Our proposed genetically optimized variational approach provides a robust method to enhance sensing performance in practical QSNs, advancing the state-of-the-art in distributed sensing applications. In future work, we aim to extend our comparisons beyond GHZ and VPS baselines by incorporating additional factors such as sample complexity, iteration number, and broader algorithmic configurations. This will provide a more comprehensive benchmarking framework and further validate the scalability and robustness of the proposed approach.

Acknowledgment

This work was supported by the National Research Foundation of Korea (NRF) grant funded by the Korean government (MSIT) (RS-2025-00556064) and by the MSIT (Ministry of Science and ICT), Korea, under the ITRC (Information Technology Research Center) support program (IITP-2025-2021-0-02046) supervised by the IITP (Institute for Information & Communications Technology Planning & Evaluation).

References

[1] U. Khalid, M. S. Ulum, A. Farooq, T. Q. Duong, O. A. Dobre, and H. Shin, "Quantum semantic communications for Metaverse: Principles and challenges," *IEEE Wireless Commun.*, vol. 30, no. 4, pp. 26–36, Aug. 2023.

[2] F. Zaman, U. Khalid, T. Q. Duong, H. Shin, and M. Z. Win, "Quantum full-duplex communication," *IEEE J. Sel. Areas Commun.*, vol. 41, no. 9, pp. 2966–2980, Sep. 2023.

[3] X. Zhao, Y. Yang, and G. Chiribella, "Quantum metrology with indefinite causal order," *Phys. Rev. Lett.*, vol. 124, no. 19, p. 190503, May 2020.
[4] U. Khalid, J. u. Rehman, S. N. Paing, H. Jung, T. Q. Duong, and H. Shin, "Quantum network engineering in the NISQ age: Principles, missions, and challenges," *IEEE Netw.*, vol. 38, no. 1, pp. 112–123, Jan. 2024.
[5] M. Cerezo, A. Arrasmith, R. Babbush, S. C. Benjamin, S. Endo, K. Fujii, J. R. McClean, K. Mitarai, X. Yuan, L. Cincio, and P. J. Coles, "Variational quantum algorithms," *Nat. Rev. Phys.*, vol. 3, no. 9, pp. 625–644, Aug. 2021.
[6] U. Khalid, J. ur Rehman, and H. Shin, "Metrologically resourceful multipartite entanglement under quantum many-body effects," *Quantum Sci. Technol.*, vol. 6, no. 2, p. 025007, Jan. 2021.
[7] B. Koczor, S. Endo, T. Jones, Y. Matsuzaki, and S. C. Benjamin, "Variational-state quantum metrology," *New J. Phys.*, vol. 22, no. 8, p. 083038, Aug. 2020.
[8] J. Liu, H. Yuan, X.-M. Lu, and X. Wang, "Quantum Fisher information matrix and multiparameter estimation," *J. Phys. A-Math. Theor.*, vol. 53, no. 2, p. 023001, Dec. 2019.
[9] J. J. Meyer, "Fisher information in noisy intermediate-scale quantum applications," *Quantum*, vol. 5, p. 539, Sep. 2021.
[10] T. Rindell, B. Yenilen, N. Halonen, A. Pönni, I. Tittonen, and M. Raasakka, "Exploring the optimality of approximate state preparation quantum circuits with a genetic algorithm," *Phys. Lett. A*, vol. 475, p. 128860, Jul. 2023.
[11] M. Schuld, V. Bergholm, C. Gogolin, J. Izaac, and N. Killoran, "Evaluating analytic gradients on quantum hardware," *Phys. Rev. A*, vol. 99, no. 3, p. 032331, Mar. 2019.
[12] R. Sweke, F. Wilde, J. Meyer, M. Schuld, P. K. Faehrmann, B. Meynard-Piganeau, and J. Eisert, "Stochastic gradient descent for hybrid quantum-classical optimization," *Quantum*, vol. 4, p. 314, Aug. 2020.
[13] D. P. Kingma and J. Ba, "Adam: A method for stochastic optimization," *arXiv:1412.6980*, Jan. 2017.
[14] L. Bittel and M. Kliesch, "Training variational quantum algorithms is NP-hard," *Phys. Rev. Lett.*, vol. 127, no. 12, p. 120502, Sep. 2021.
[15] J. Romero, R. Babbush, J. R. McClean, C. Hempel, P. J. Love, and A. Aspuru-Guzik, "Strategies for quantum computing molecular energies using the unitary coupled cluster ansatz," *Quantum Sci. Technol.*, vol. 4, no. 1, p. 014008, Oct. 2018.
[16] S. Y.-C. Chen, C.-M. Huang, C.-W. Hsing, H.-S. Goan, and Y.-J. Kao, "Variational quantum reinforcement learning via evolutionary optimization," *Mach. Learn.-Sci. Technol.*, vol. 3, no. 1, p. 015025, Feb. 2022.
[17] T. Baumgratz and A. Datta, "Quantum enhanced estimation of a multidimensional field," *Phys. Rev. Lett.*, vol. 116, no. 3, p. 030801, Jan. 2016.